INTERNATIONAL JOURNAL FOR NUMERICAL METHODS IN FLUIDS
Int. J. Numer. Meth. Fluids 2002; **40**:1327–1346 (DOI: 10.1002/fld.421)

Effect of rotation on Goertler vortices in the boundary layer flow on a curved surface

C. T. Chen[1] and M. H. Lin[2,*,†]

[1]*Department of Industrial Engineering and Management, Ta-Hwa Institute of Technology, Hsinchu 307, Taiwan, ROC*
[2]*Department of Automation Engineering, Ta-Hwa Institute of Technology, Hsinchu 307, Taiwan, ROC*

SUMMARY

This paper presents a numerical prediction of the formation of Goertler vortices on a curved surface with effect of rotation. The criterion of flow visualization marking the onset position of Goertler vortices is employed in the present paper. For facilitating the numerical study, the computation is carried out in the transformed x and η plane. The results show that the onset position characterized by the Goertler number, depends on the rotation number Ro, the Prandtl number and the wave number. The value of critical Goertler number increases with the increase in negative rotation, while the value of Goertler number decreases with the increase in positive rotation on a concave surface. On the contrary, the value of critical Goertler number decreases with the increase in negative rotation on a convex surface. The obtained critical Goertler number and wave number are compared with the previous theoretical and experimental data. Copyright © 2002 John Wiley & Sons, Ltd.

KEY WORDS: numerical prediction; Goertler vortices; curved surface; rotation

1. INTRODUCTION

The study of Goertler vortices on a curved wall with the effect of rotation is of practical significance for its engineering applications. The Goertler vortices change flow properties, such as wall friction, heat transfer rate, and separation characteristics, etc. It is important when engineers design a practical curved plate in a given flow to ensure the laminar flow control. They also strongly increase the heat transfer in the boundary layer on cooled walls as in turbine blades. Moreover, the boundary layers developed on curved blades in turbo-machineries are subjected to rotation. The studies on the Goertler vortices were reviewed by Herbert [1], and Floryan [2]. Only a few studies on the Goertler vortices on a curved surface with the effect of rotation were discussed by Aouidef *et al.* [3], Zebib and Bottaro [4] and

* Correspondence to: M. H. Lin, Department of Automation Engineering, Ta-Hwa Institute of Technology, Hsinchu 307, Taiwan, ROC.
† E-mail: aemhlin@et4.thit.edu.tw

Contract/grant sponsor: National Science Council; contract/grant number: NSC89-2212-E233-009

Received August 2001
Revised 6 April 2002

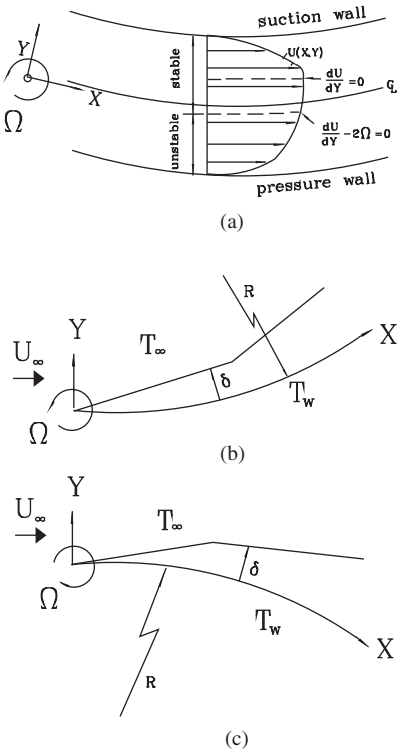

Figure 1. Physical configuration and curvilinear co-ordinate system: (a) rotating curved channel; (b) rotating concave surface; and (c) rotating convex surface.

Edo *et al*. [5], etc. The obtained theoretical values are seen two orders of magnitude below the corresponding experimental data. By reviewing the criteria of the onset of the longitudinal vortices in boundary layer and channel flows, the experimental and numerical methods employed in the literature for determining the onset of longitudinal vortices were summarized in Reference [6]. Moreover, the study of the formation of longitudinal vortices in a boundary layer flow with rotation on a flat plate has been studied by the authors [7]. Some laboratory data with rotation effect have been compared to verify the proposed model.

Several studies were focused on the vortex instability in rotating curved channel flows (for example, Mutabazi *et al.* [8], Matsson and Alfredsson [9], Selmi *et al.* [10], Matsson and Alfredsson [11], Wang and Cheng [12], Wang [13], etc.). Although these studies of the rotating curved channel flow can be regarded as qualitative references, there are several important differences between the rotating curved boundary layer and curved channel flows. The curved channel flow is consisted of the stable layer on the suction wall and the unstable layer on the pressure wall, as shown in Figure 1(a). These two layers are directly adjacent to each other resulting in the interaction between the opposite effects of Coriolis force at the interface. Depending on the direction of rotation, destabilizing effects due to the curvature and the rotation may either enhance or counteract each other. However, the potential flow and the wall bound the rotating curved boundary layer. In consequence, non-linear interaction

of centrifugal force and Coriolis force stabilizes or destabilizes the curved boundary layer according to the direction of rotation and positive (or negative) curvature. The complicated flow structure induced by these two destabilizing mechanism can be observed independently.

It is noted that the theoretical investigations in the literature on the onset of Goertler vortices on the curved boundary layer flow with the effect of rotation are rather limited and incomplete. The work was motivated by a desire to explore the extent of destabilization/stabilization of the Blasius flow on a curved surface for the formation of Goertler vortices with the effect of rotation. The experimental criteria proposed by Hwang and Lin [6] marking the onset of longitudinal vortices were employed in the present study. The governing parameters for the effect of rotation on the onset of Goertler vortices are the rotation number $Ro=\Omega R/U_\infty$, Prandtl number, and the wave number a. In the computation, the Prandtl number is 0.7 (for air), the magnitudes of imposed initial disturbance velocity $u^0=10^{-3}$, and the rotation number $Ro=-12$ to 12.

2. THEORETICAL ANALYSIS

Consider a laminar Blasius flow on a curved wall with a free stream velocity U_∞. As shown in Figure 1(b) and 1(c), the physical curvilinear co-ordinates are chosen such that X measures the streamwise distance from the leading edge of the curved wall, Y is the distance normal to the wall, and Z is in the transverse direction. The present study assumes constant fluid thermophysical properties, large radius of curvature R of a curved wall and large Reynolds number. The basic flow and energy equations in similarity forms $f'''+ff''/2=0$ and $\theta_b''+\Pr f\theta_b'/2=0$ can be found readily in many texts, where $f(\eta)=\psi(vXU_\infty)^{-1/2}$, $\theta_b(\eta)=(T-T_\infty)/(T_w-T_\infty)$ and $\eta=Y(vX/U_\infty)^{-1/2}$. The similarity solutions of the basic quantities will be used to compute the solution of perturbation equations. The boundary layer equation governing the basic flow along a rotating curved surface is reduced to that of stationary boundary layer (Blasius flow) if the static pressure on the wall is kept constant. The free stream condition should be modified because of non–zero relative vorticity in the free stream. For this reason, the Blasius profile is modified by simply adding $2\Omega Y$, i.e.

$$\bar{U}=\bar{U}_{\text{Blasius}}+2\Omega Y \quad \text{(dimensional form) or}$$

$$f'=f'_{\text{Blasius}}+2\frac{\Omega R}{U_\infty}Re^{-1/2}y=f'_{\text{Blasius}}+2Ro\,Re^{-1/2}\sqrt{x}\eta \quad \text{(dimensionless form).} \tag{1}$$

The other boundary conditions are $f'(0)=\theta_b(0)-1=f'(\infty)-1=\theta_b(\infty)=0$.

In the region near or upstream of the onset position x^*, the disturbances of longitudinal vortex type are small and the non-linear terms in the momentum and energy equations may be linearized. Furthermore, in experiments [14–19] 'stationary' longitudinal vortex rolls have been found periodic with a wave length λ in the transverse direction Z. Therefore, the disturbances superimposed on the two-dimensional basic flow quantities can be expressed as

$$\begin{aligned} G(X,Y,Z)&=G_b(X,Y)+\zeta(X,Y)\exp(ia'Z)\\ W(X,Y,Z)&=w'(X,Y)i\exp(ia'Z)\end{aligned} \tag{2}$$

where $G=U,V,P$ or T, $\zeta=\mathrm{u}',\mathrm{v}',\mathrm{p}'$ or t'. The value $a'=2\pi/\lambda$ is the dimensional transverse wave number of the vortex rolls. By consideration of the vortex-type perturbation quantities in continuity equation, a different expression for W is used.

Substituting Equation (2) into the continuity, Navier–Stokes, and energy equations in curvilinear co-ordinates, and subtracting the two-dimensional basic flow and energy equations under the assumptions of $Re \gg 1$, $Ro \sim O(1)$ and $R \gg 1$, one can obtain the linearized perturbation equations.

$$\frac{\partial u'}{\partial x}+\frac{\partial v'}{\partial y}-a'w'=0 \tag{3}$$

$$U_\mathrm{b}\frac{\partial u'}{\partial X}+u'\frac{\partial U_\mathrm{b}}{\partial X}+V_\mathrm{b}\frac{\partial u'}{\partial Y}+v'\frac{\partial U_\mathrm{b}}{\partial Y}=\frac{\mu}{\rho}\nabla^2 u' \tag{4}$$

$$U_\mathrm{b}\frac{\partial v'}{\partial X}+u'\frac{\partial V_\mathrm{b}}{\partial X}+V_\mathrm{b}\frac{\partial v'}{\partial Y}+v'\frac{\partial V_\mathrm{b}}{\partial Y}=\frac{\mu}{\rho}\nabla^2 v'-\frac{1}{\rho}\frac{\partial p'}{\partial Y}-\frac{2}{R}U_\mathrm{b}u'-2\Omega u' \tag{5}$$

$$U_\mathrm{b}\frac{\partial w'}{\partial X}+V_\mathrm{b}\frac{\partial w'}{\partial Y}=\frac{\mu}{\rho}\nabla^2 w'-\frac{1}{\rho}a'p' \tag{6}$$

$$U_\mathrm{b}\frac{\partial t'}{\partial X}+u'\frac{\partial T_\mathrm{b}}{\partial X}+V_\mathrm{b}\frac{\partial t'}{\partial Y}+v'\frac{\partial T_\mathrm{b}}{\partial Y}=\alpha\nabla^2 t' \tag{7}$$

where $\nabla^2=(\partial^2/\partial Y^2)-a'^2$ is a two-dimensional Laplacian operator. The perturbation equations are two-dimensional and of boundary layer flow type.

Next, one introduces the following dimensionless variables and parameters:

$$\begin{gathered}
X=Rx,\quad [Y\quad Z]=R\,Re^{-1/2}[y\quad z]\\
[U_\mathrm{b}\quad u']=U_\infty[\bar{u}\quad u],\quad [V_\mathrm{b}\quad v'\quad w']=U_\infty\,Re^{-1/2}[\bar{v}\quad v\quad w]\\
[T_\mathrm{b}-T_\infty\quad t']=(T_\mathrm{w}-T_\infty)[\theta_\mathrm{b}\quad t],\quad p'=\frac{\rho U_\infty^2}{Re}p,\quad a'=\frac{Re^{1/2}}{R}a\\
Re=\frac{\rho U_\infty R}{\mu},\quad Ro=\frac{\Omega R}{U_\infty}
\end{gathered} \tag{8}$$

and a vorticity function in the axial direction

$$\xi=\frac{\partial w}{\partial y}-\frac{\partial v}{\partial z}=\frac{\partial w}{\partial y}-av \tag{9}$$

To obtain equation for the vorticity, one may differentiate Equations (5) and (6) by z and y, respectively, and then eliminate the pressure terms by subtracting one from another. To derive the equation for v, one may differentiate Equation (9) with respect to z. Similarly, the equation for w can be obtained by differentiating Equation (9) by y. It is noted that in the derivation of equations for v and w, continuity Equation (3) must be considered. By using also the similarity variable $\eta=y/\sqrt{x}$, the perturbation equations in η and x plane are found.

$$\frac{\partial^2 u}{\partial\eta^2}+\frac{1}{2}f\frac{\partial u}{\partial\eta}-xf'\frac{\partial u}{\partial x}-a^2xu+\frac{1}{2}\eta f''u=f''\sqrt{x}v \tag{10}$$

$$\frac{\partial^2 t}{\partial \eta^2} + \frac{1}{2} Pr\, f \frac{\partial t}{\partial \eta} - xPrf' \frac{\partial t}{\partial x} - a^2 xt = Pr \frac{\partial \theta_b}{\partial \eta} \left(-\frac{1}{2}\eta u + \sqrt{x} v \right) \tag{11}$$

$$\frac{\partial^2 \xi}{\partial \eta^2} + \frac{1}{2} f \frac{\partial \xi}{\partial \eta} - xf' \frac{\partial \xi}{\partial x} - \left(\frac{1}{2}\eta f'' + a^2 x \right) \xi = -2xa\, Re^{1/2} K(f' + Ro)u$$
$$-au \left(\frac{1}{4\sqrt{x}} (f - \eta f' - \eta^2 f'') \right) + \sqrt{x} f'' \left(\frac{\partial w}{\partial x} - \frac{\eta}{2x} \frac{\partial w}{\partial \eta} \right) \tag{12}$$

$$\frac{\partial^2 v}{\partial \eta^2} - xa^2 v = ax\xi - \sqrt{x} \frac{\partial^2 u}{\partial x \partial \eta} + \frac{\eta}{2\sqrt{x}} \frac{\partial^2 u}{\partial \eta^2} + \frac{1}{2\sqrt{x}} \frac{\partial u}{\partial \eta} \tag{13}$$

$$\frac{\partial^2 w}{\partial \eta^2} - xa^2 w = \sqrt{x} \frac{\partial \xi}{\partial \eta} - ax \frac{\partial u}{\partial x} + \frac{1}{2} a\eta \frac{\partial u}{\partial \eta} \tag{14}$$

where $K = +1$ in Equation (12) for concave curvature and $K = -1$ for convex curvature. It is noted that the first term on the right hand side of Equation (12) is the major driving force of Goertler vortices (both centrifugal force and Coriolis force are coupled). The set of equations (5)–(9) is a boundary value problem in the η-direction, an initial value problem in the x-direction, and an eigenvalue problem in the z-direction. The appropriate initial condition and boundary conditions of the perturbations equations are

$$\begin{aligned} &u = v = w = t = 0 \quad \text{at } \eta = 0 \\ &u = v = w = t = \xi = 0 \quad \text{at } \eta = \infty \\ &u - u^0 = v = w = \xi = t = 0 \quad \text{at } x = 0 \end{aligned} \tag{15}$$

For simplicity, the initial amplitude function u^0 is set uniform, and the other two velocity components v and w are set zero. However, the magnitudes of the velocities v and w will be generated in the next x-steps. The range of the initial amplitude function, $u^0 = 10^{-3}$ is used in the present study. In the experiment of Swearingen and Blackwelder [18], the free stream turbulence level in their well controlled wind tunnel was less than 0.07% that corresponding to the perturbation velocity u with magnitude between 10^{-4} and 10^{-3}.

Equations (10)–(14) and boundary conditions (15) in the $x - \eta$ plane are for unknowns u, t, ξ, v and w with three fixed values of a, Ro and Re. By giving a series value of a and Ro, the largest amplification of the perturbation quantities along the x-direction determines the value of critical wave number a^*. One can see that the term $-2xa\, Re^{1/2} f'u$ on the right-hand side of Equation (12) may be expressed as $-2(x^{1/2}a)(x\, Re)^{1/2} f'u$ in which $(x^{1/2}a)$ is the dimensionless wave number defined by using the characteristic boundary layer thickness, and $x\, Re = \rho U_\infty X/\mu$ is the local Reynolds number. The radius of curvature does not appear explicitly in Equations (10)–(14). One may prove analytically the homogeneity of R in Equations (10)–(14) by considering the dimensionless transformations (8) i.e. $v \sim R^{1/2}$, $w \sim R^{1/2}$, $a \sim R^{1/2}$, $x \sim R^{-1}$, $y \sim R^{-1/2}$, $z \sim R^{-1/2}$, and $\xi \sim R$ (variables of u, η, and f are independent of R). In the computation, the selection of Re does not change the local critical Reynolds number $(xRe)^*$ and the critical wave number $(x^{1/2}a)^*$. This is also proved by using several values of Re in computation. The present study, $Re^{1/2} = 250$ is used for demonstrating the results.

The local friction factor and the local Nusselt number of the basic and perturbed flows can be also expressed, respectively, as

$$C_{fX} = C_{fb} + C_{fp} = \frac{\tau_{wb} + \tau_{wp}}{(1/2)\rho U_\infty^2} = 2\,Re_X^{-1/2}\left[f''(0) + \left.\frac{\partial u}{\partial \eta}\right|_w\right]$$

or

$$\frac{C_{fX}}{C_{fb}} = 1 + \left.\frac{\partial u}{\partial \eta}\right|_w \Big/ f''(0) \tag{16}$$

and

$$Nu_X = Nu_b + Nu_p = \frac{(h_b + h_p)X}{k} = -Re_X^{1/2}\left[\theta_b'(0) + \left.\frac{\partial t}{\partial \eta}\right|_w\right]$$

or

$$\frac{Nu_X}{Nu_b} = 1 + \left.\frac{\partial t}{\partial \eta}\right|_w \Big/ \theta_b'(0) \tag{17}$$

where τ_w and h are the local wall shear stress and local heat transfer coefficient, respectively, the subscripts b and p indicate the basic and perturbed flows, and k is the fluid thermal conductivity. Noted that the Nu_X is based on the thermal boundary condition of constant wall temperature.

3. NUMERICAL PROCEDURE

A finite difference scheme based on the weighting function Lee [20] with second order accuracy in both η and x is used. The step-by-step procedure is listed as follows.

(1) Assign $Pr, Re^{1/2}$ and Ro to obtain the basic flow and temperature distributions. The value of Pr is 0.7, $Re^{1/2} = 250$, and the values of Ro are -0.9 to 12 for concave wall and $Ro = -0.1$ to -12 for convex wall in the present study.

(2) Assign zero initial values of v, w, ξ and t, initial velocity at leading edge, $u^0 = 10^{-3}$ and various values of wave number a.

(3) Solve Equations (10)–(12) for u, t and ξ distributions at the next x-step. Values of ξ on boundary are evaluated with previous iteration data of v and w in the interior region.

(4) Solve Equations (13) and (14) for v and w with the obtained u and ξ.

(5) Repeat steps (3) and (4), until the perturbation quantities meet the convergence criteria at the streamwise position.

$$\text{Max}\left(\frac{|g_{i,j}^{(n+1)}| - |g_{i,j}^{(n)}|}{g_{i,j}^{(n+1)}}\right) \leqslant 10^{-5} \tag{18}$$

where $g_{i,j}^{(n)}$ are the perturbation quantities u, v, w, t and ξ of nodal point (i, j) at the nth number of iteration.

(6) Calculate the local friction factor and the local Nusselt number of the vortex flow.

(7) Repeat steps (3)–(6) at the next mainstream position until a desired mainstream position is reached.
(8) The absolute values of perturbation quantities are growing along the mainstream direction. One can find the mainstream position marked with the subscript i, where the flow visualization onset criterion $Y_i = \int_0^{X^*} \mathrm{Max}|v'| \dfrac{\mathrm{d}X}{U_\infty} = 2$ mm or $y_i = \int_0^{x^*} \mathrm{Max}_j |v_{i,j}^{(n)}| \,\mathrm{d}x = 0.002$ is satisfied, where Y_i is the detectable height of vortex spike.

Various onset positions x_{cr} can be determined for different values of wave number a. The value of a is assigned in the computation, where the range of $a = 0.2$–3.5 and step $= 0.02$. The minimum x_{cr} denoted by x^* is the most probable onset position and the corresponding wave number is denoted by a^*. The local critical Goertler number is $G_X^* = 2x^{*3/2}Re^{1/2}$ and the local wave number is $a^*x^{*1/2}$ for this computation.

The criterion for determination of the onset of longitudinal vortices using the technology of flow visualization in experiments can be explained as follows:

Flow visualization is one of the most effect methods in determining the onset of longitudinal vortices in boundary and channel flows. There are several flow visualization techniques that can be applied, e.g. electrochemical techniques, smoke dye, and particle techniques, and optical methods. Among these flow visualization techniques, smoke flow visualization is used quite frequently in boundary and channel flow for air [21–26]. Usually, a light slit is set in a direction normal to the streamwise direction to observe the smoke distribution. The smoke particles are injected at the same Y at inlet and may be periodically distributed along the transverse direction if the longitudinal vortices appear. Let the detectable fluctuation displacement of the smoke in Y direction be ΔY, then

$$\Delta Y_i = \int_0^{\tau} v' \,\mathrm{d}\tau = \int_0^{X^*} \mathrm{Max}|v'| \frac{\mathrm{d}X}{U_\infty} \quad \text{or} \quad \Delta y_i = \int_0^{x^*} \underset{j}{\mathrm{Max}} |v_{i,j}^{(n)}| \,\mathrm{d}x \tag{19}$$

where τ is the time elapsed for fluid flow from inlet along the streamwise direction, and v' and v are the dimensional and dimensionless normal direction perturbation velocities, respectively. Typically, the onset criterion based on smoke flow visualization is $\Delta\mathrm{Y} = 0.002$ m. Also, by comparison of the onset criterion between $\Delta y_i = 0.002$ and $\Delta y_i = 0.003$ in the numerical experiment, the values of onset position x^* increases less than 5%. Moreover, by comparison of the onset criterion between $\Delta y_i = 0.002$ and $\Delta y_i = 0.004$ in the numerical experiment, the values of onset position x^* increases less than 10%. It is reasonable to set $\Delta y_i = \int_0^{x^*} \mathrm{Max}_j |v_{i,j}^{(n)}| \,\mathrm{d}x = 0.002$ in the numerical solution for the onset criterion of Goertler vortices.

The grids are tested for various Δx and $\Delta\eta$ are listed in Table I. A grid size of $\Delta x = 0.002$, $\Delta\eta = 0.02$ and $\eta_\infty = 10$ is used within 0.2% error to perform the numerical experiment in the present study. To check the validity of the linear Equations (10)–(14), the order of magnitude of non-linear terms of perturbation equations near the onset position are checked. The calculated data are substituted into the individual terms of the x-momentum equation. The orders of the non-linear terms is two orders of magnitude smaller than the order of linearized inertia terms. Therefore, the linear theory is valid for the estimation of the onset of Goertler vortices.

Table I. Grid size test for $Re^{1/2}=250$, $a^*=1.34$, $Pr=0.7$ and $Ro=0$.

Δx	$\Delta\eta$	$x=0.1$	0.2	0.3	0.4	0.5
0.002	0.02	0.01437[a]	0.04952	0.2413	1.733	16.05
0.002	0.01	0.01437	0.04952	0.2412	1.732	16.04
0.001	0.02	0.01431	0.04942	0.2408	1.730	16.02

[a] These are the maximum values of mainstream velocity $u/0.01$ at the specified x position.

4. RESULTS AND DISCUSSION

The typical development of the dimensionless perturbation amplitudes u, v, w, and t at $x=0.35$, 0.4, 0.45, and 0.5 for $Pr=0.7$, $Re^{1/2}=250$, $a^*=1.34$, and $Ro=0$ is shown in Figure 2. The magnitude of v and w are larger than those of u and t because the scaling factor $Re^{-1/2}$ is included in these quantities. The shapes of the v and w profiles may be regarded as a vortex pattern. This figure also presents the development of the perturbation amplitude quantities in the streamwise direction.

Figure 3 depicts the dimensionless perturbation amplitude functions at $x=0.8$, 0.9, 1.0, 1.1, and 1.2 with negative rotation $Ro=-0.5$. It is seen that the values of perturbation amplitude functions are decreased with the stabilizing effect of Coriolis force. It is also observed in this figure that the profiles of perturbation amplitude functions are shrunk to smaller η region due to the rotation effect. On the contrary, as shown in Figure 4, the values of perturbation function are increased, and the sizes of function are enlarged to larger η region with positive rotation $Ro=2$. It is noted that positive rotation destabilizes the flow, as the Coriolis force acts in the same direction as the centrifugal force.

Figures 5 and 6 depict the typical development of the dimensionless perturbation amplitudes u, v, w, and t on a convex surface. It is shown that the values of perturbation amplitude functions are decreased downstream of convex surface with zero rotation, due to the centrifugal force stabilizes the flow. On the contrary, as shown in Figure 6, the values of perturbation function are increased, and the sizes of function are enlarged to larger η region with negative rotation $Ro=-2$ on a convex surface with the destabilizing effect of Coriolis force.

It is interesting to study numerically the variations of friction factor and heat transfer coefficient after the onset of Goertler vortices. The perturbation friction factor C_{fp} and heat transfer rate Nu_{p} behaves like a cosine function in the Z-direction (i.e. $C_{\mathrm{f}} \propto \partial U/\partial Y \propto \exp(\mathrm{i}a'Z)$ and $Nu \propto \partial T/\partial Y \propto \exp(\mathrm{i}a'Z)$). Although the mean values of friction factor and heat transfer rate in one spanwise wave is zero, the maximum variation of local heat transfer rate along z-direction occurred at $z=0$ and $2\pi/a$. The variations of local $C_{\mathrm{f}X}/C_{\mathrm{fb}}$ and Nu_X/Nu_{b} along the axial direction at $z=0$ are shown in Figure 7(a) and Figure 7(b), respectively. The friction factor coefficient for the turbulent boundary layer flow based on the one-seventh power law velocity profile [27] is

$$C_{\mathrm{f}X} \approx 0.027 Re_X^{-1/7} \quad \text{or} \quad C_{\mathrm{f}X} Re^{1/2} \approx 0.027 Re_X^{5/14} = 0.027[(G_X Re/2)^{2/3}]^{5/14} \tag{20}$$

or

$$C_{\mathrm{f}X}/C_{\mathrm{fb}} = 0.081[(G_X Re/2)^{2/3}]^{5/14}$$

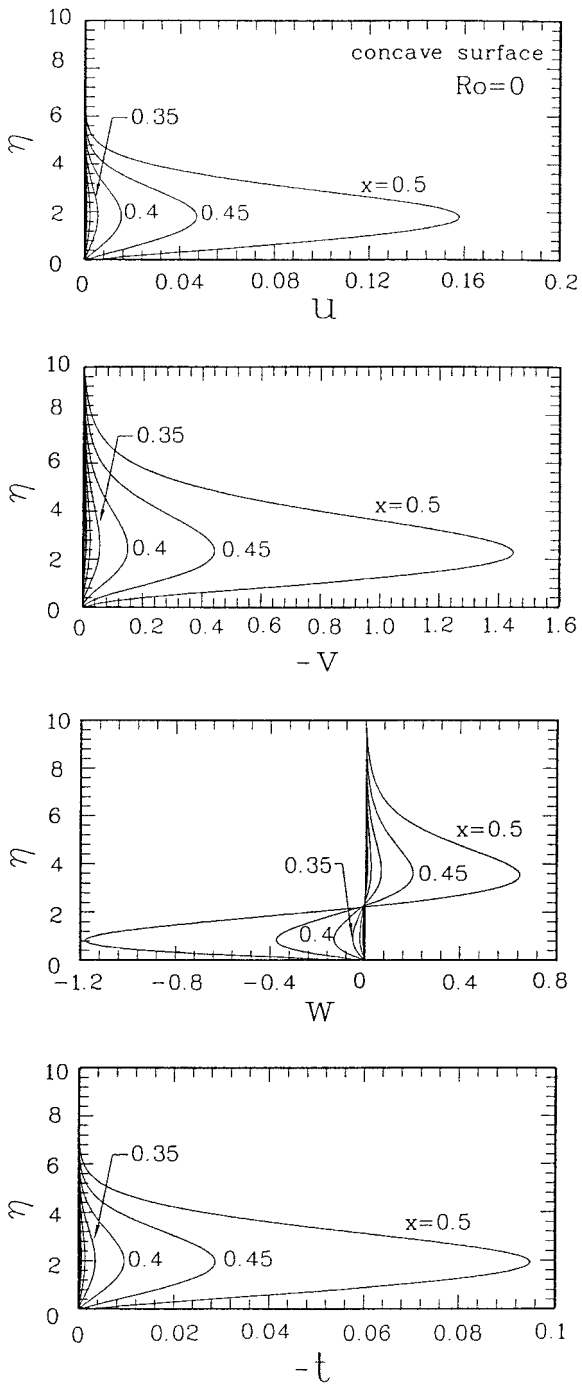

Figure 2. Development of perturbation amplitude profiles at specified x positions for $Ro=0$ on a concave surface ($Pr=0.7$, $Re^{1/2}=250$ and $a^* = 1.34$).

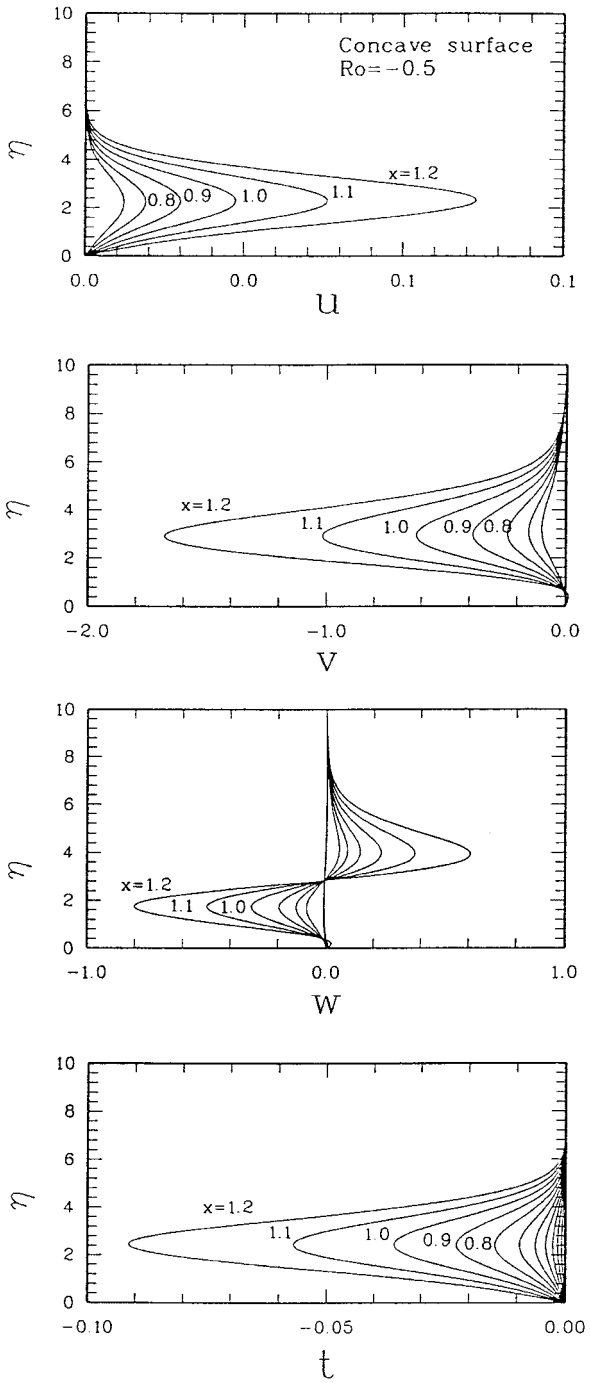

Figure 3. Development of perturbation amplitude profiles at specified x positions for $Ro=-0.5$ on a concave surface ($Pr=0.7$, $Re^{1/2}=250$ and $a^*=1.34$).

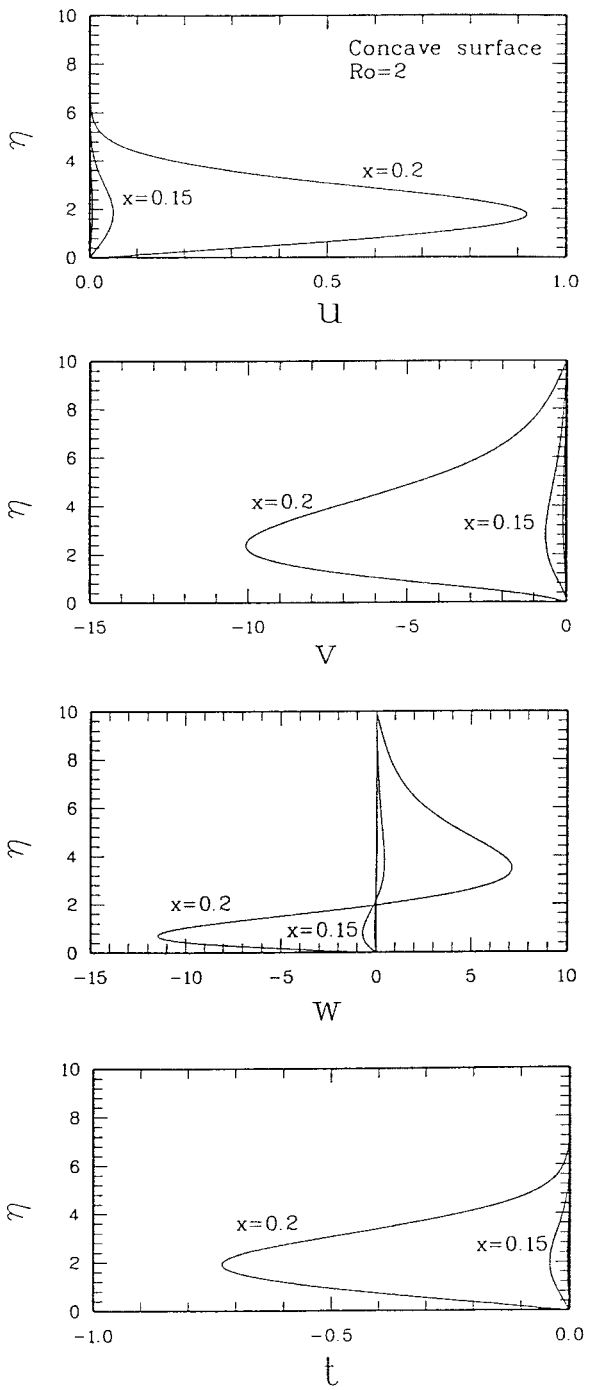

Figure 4. Development of perturbation amplitude profiles at specified x positions for $Ro=2$ on a concave surface ($Pr=0.7$, $Re^{1/2}=250$ and $a^*=1.34$).

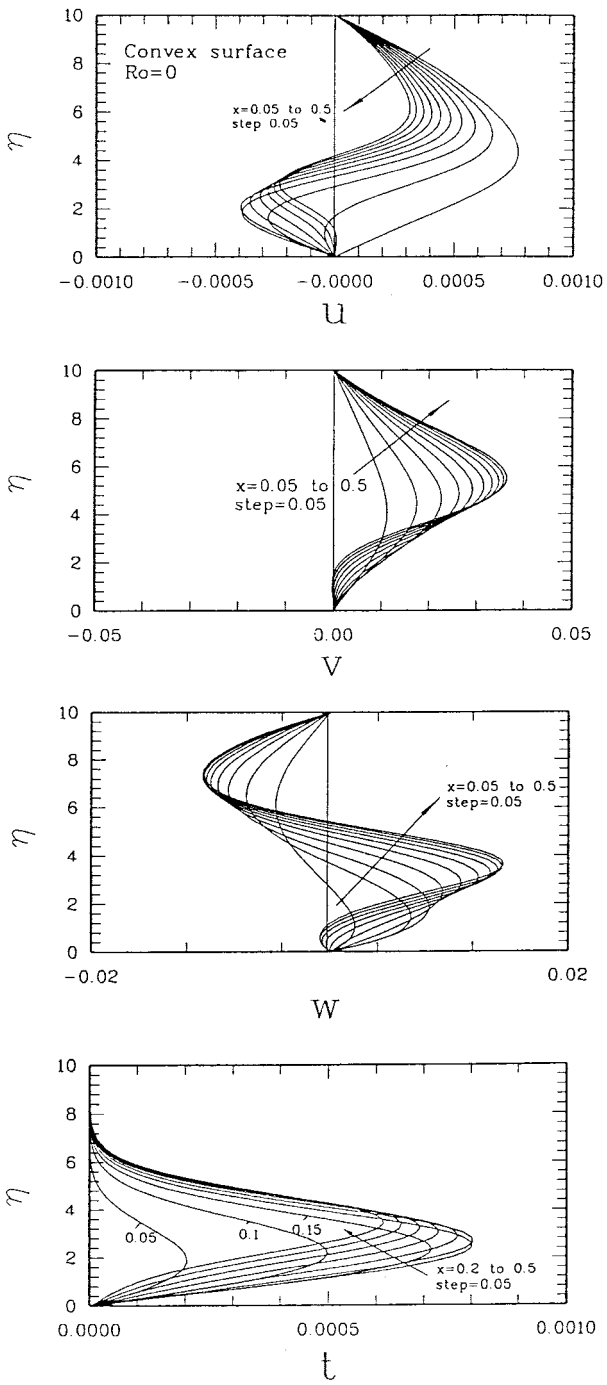

Figure 5. Development of perturbation amplitude profiles at specified x positions for $Ro=0$ on a convex surface ($Pr=0.7$, $Re^{1/2}=250$ and $a^*=2.0$).

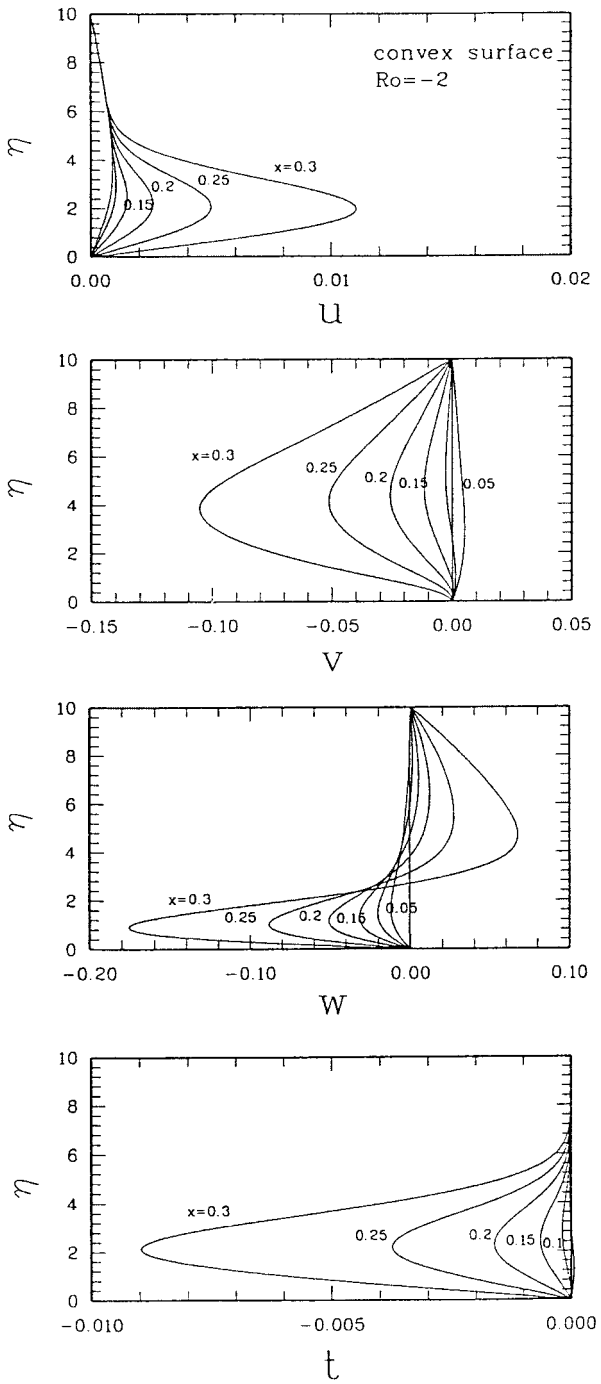

Figure 6. Development of perturbation amplitude profiles at specified x positions for $Ro=-2$ on a convex surface ($Pr=0.7$, $Re^{1/2}=250$ and $a^*=2.0$).

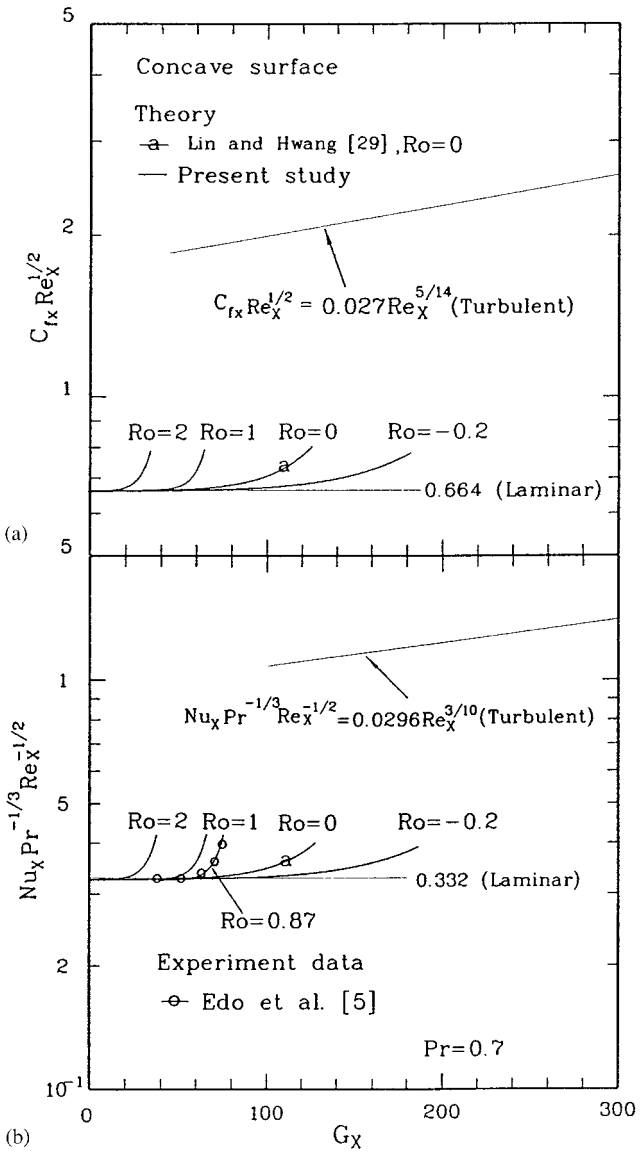

Figure 7. (a) Friction factor and (b) Nusselt number for $Ro = -0.2$, 0, and 2 on a concave surface.

and the correlation equation for turbulent forced convection [28] is

$$Nu_X = 0.0296 Re_X^{4/5} Pr^{1/3} \quad \text{or}$$

$$Nu_X Pr^{-1/3} Re_X^{-1/2} = 0.0296 Re_X^{3/10} = 0.0296[(G_x Re/2)^{2/3}]^{3/10} \tag{21}$$

Table II. Onset position x^* for criterion $y_i = \int_0^{x^*} \mathrm{Max}_j |v_{i,j}^{(n)}| \, \mathrm{d}x = 0.002$ on a concave surface.

Ro	x^*	G_X^*	$a^* x^{*1/2}$
−0.9	0.560	209.5	1.0
−0.7	0.306	84.6	0.74
−0.5	0.222	52.3	0.63
−0.3	0.182	38.8	0.57
−0.2	0.168	34.4	0.55
0.0	0.162	32.6	0.54
1	0.106	17.3	0.44
2	0.088	13.0	0.40
4	0.070	9.3	0.35
6	0.060	7.3	0.33
8	0.054	6.3	0.31
10	0.050	5.6	0.30
12	0.046	4.9	0.29

Note—These values are evaluated by using $Re^{1/2} = 250$, $a^* = 1.34$, $Pr = 0.7$ and $u^0 = 10^{-3}$.

or

$$Nu_X / Nu_\mathrm{b} = 0.089[(G_X Re/2)^{2/3}]^{3/10}$$

where $f''(X,0) = 0.332$ and $-\theta_\mathrm{b}'(X,0) = 0.332$ of Blasius flow at $Ro = 0$ and $Pr = 0.7$ are chosen for reference.

The friction factor and the Nusselt number are also shown for comparison. The gradients of the velocity and the temperature at the wall start to deviate from the laminar forced convection at downstream of x^*, due to the secondary longitudinal vortex flow on the heated concave wall. The effect of rotation on Goertler vortices are more pronounced when the values of rotation number is decreased/increased, as compared with zero rotation. Similar observations were also made by Edo *et al.* [5].

The critical values of G_X^* and the local critical wave number $a^* x^{*1/2}$ may be converted to G_θ^* and $a'^* \theta$, respectively, by the following transformations:

$$G_\theta^* = \frac{U_\infty \theta}{\nu} \sqrt{\frac{\theta}{R}} = [(0.664)^3 G_X^*/2]^{1/2} \tag{22}$$

and

$$(a'\theta)^* = \left(\frac{2\pi}{\lambda} \frac{0.664X}{Re_X^{1/2}} \right)^* = 0.664(ax^{1/2})^* \tag{23}$$

where the momentum thickness $\theta = 0.664X/Re_X^{1/2}$. The effect of rotation on the critical Goertler number G_X^* on a concave surface is listed in Table II and Figure 8. It is observed from the data that a decrease in the rotation number Ro from 0 to −0.9 is to increase up to 6.4 times the value of critical Goertler number G_X^*. For negative rotation the Coriolis force counteracts the centrifugal force and increases the critical Goertler number. While an increase in the rotation number Ro from 0 to 12 is to decrease G_X^* by 0.15 times. It is clear that positive

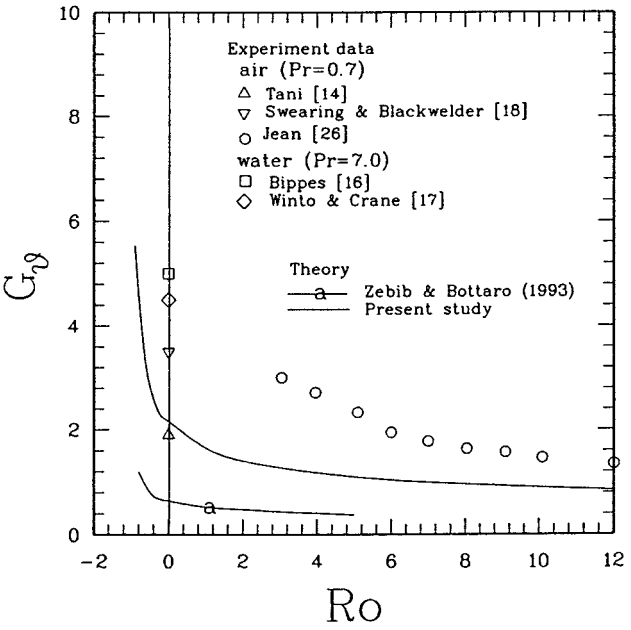

Figure 8. The relation between the critical values G_θ^* and Ro on a concave surface.

Table III. Onset position x^* for criterion $y_i = \int_0^{x^*} \mathrm{Max}_j|v_{i,j}^{(n)}|\,\mathrm{d}x = 0.002$ on a convex surface.

Ro	x^*	G_X^*	$a^* x^{*1/2}$
−0.1	0.176	36.9	0.839
−0.3	0.166	33.8	0.815
−0.5	0.160	32.0	0.800
−0.7	0.154	30.2	0.785
−1.0	0.146	27.9	0.764
−2	0.130	23.4	0.721
−4	0.112	18.7	0.669
−6	0.100	15.8	0.632
−8	0.094	14.4	0.613
−10	0.088	13.1	0.593
−12	0.084	12.2	0.579

Note—These values are evaluated by using $Re^{1/2} = 250$, $a^* = 2.0$, $Pr = 0.7$ and $u^0 = 10^{-3}$.

rotation destabilizes the flow, as the Coriolis force acts in the same direction as the centrifugal force.

The effect of rotation on the critical Goertler number G_X^* on a convex surface is listed in Table III and Figure 9. It is observed from the data that decrease in the rotation number Ro from −0.1 to −12 is to decrease the value of critical Goertler number G_X^* by 0.33 times. This is due to the Coriolis force counteracts the centrifugal force, thus destabilizes

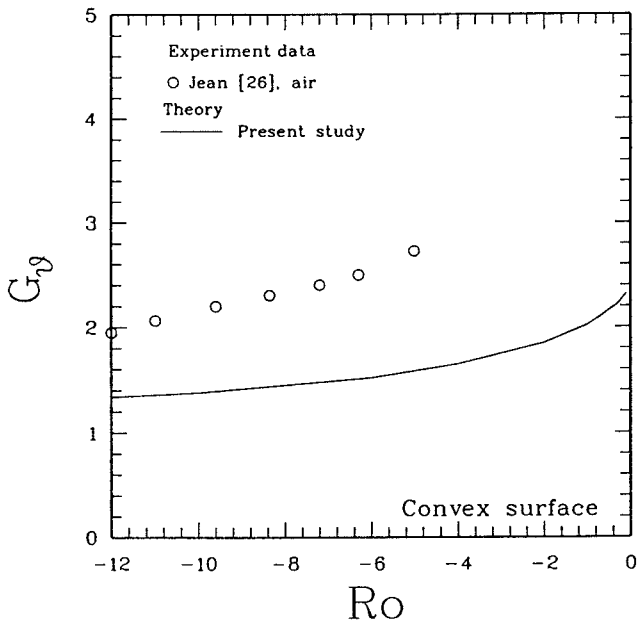

Figure 9. The relation between the critical values G_{θ}^{*} and Ro on a convex surface.

the flow. The results of the present study show a reasonable agreement with the previous experimental data [26].

5. CONCLUSIONS

1. The effect of rotation on the destabilization and stabilization of the Blasius flow on a curved surface for the formation of Goertler vortices are studied numerically by using flow visualization onset criterion and a linear instability model.
2. A decrease in the rotation number Ro from 0 to -0.9 is to increase up to 6.4 times the value of critical Goertler number G_{X}^{*} on a concave surface. While an increase in rotation number from 0 to 12 is to decrease G_{X}^{*} by 0.15 times.
3. A decrease in the rotation number Ro from -0.1 to -12 is to decrease the value of critical Goertler number G_{X}^{*} by 0.33 times on a convex surface. This is due to the Coriolis force counteracts the centrifugal force, thus destabilizes the flow. The results of the present study show a reasonable agreement with the previous experimental data.

ACKNOWLEDGEMENTS

The authors wish to express their appreciation to the National Science Council, Taiwan (Grant No. NSC89-2212-E233-009), for their encouragement and financial of this work.

NOMENCLATURE

a', a	dimensional and dimensionless wave number, $a' = a\,Re^{1/2}/R$
C_f	friction factor, $2\tau_w/\rho U_\infty^2$
F	velocity, pressure or temperature function
f	reduced stream function, $\psi(\nu X U_\infty)^{-1/2}$
G_X	local Goertler number, $2X\,Re_X^{1/2}/R$
$G_{X,\mathrm{rot}}$	local rotational Goertler number, $2(\Omega X/U_\infty)Re_X^{1/2}$
h	local heat transfer coefficient
p', p	dimensional and dimensionless pressure, $p' = \rho U_\infty^2 p/Re$
Pr	Prandtl number, ν/α
Nu_X	local Nusselt number, hX/k
R	radius of curvature (m)
Re	Reynolds number based on radius of curvature, $U_\infty R/\nu$
Re_X	local Reynolds number, $U_\infty X/\nu$
Ro	rotation number based on radius of curvature, $\Omega R/U_\infty$
T	temperature (K)
t', t	dimensional and dimensionless perturbation temperature, $t' = (T_w - T_\infty)t$
U, V, W	dimensional velocity components (m/s)
u, v, w	dimensionless perturbation velocity components
u', v', w'	perturbation velocity components
u^0	initial constant perturbation velocity at $x = 0$
X, Y, Z	Cartesian co-ordinates (m)
x, y, z	dimensionless Cartesian co-ordinates as defined in (8)

Greek letters

Ω	rotation speed (rad/s)
α	thermal diffusivity of fluid
δ	boundary layer thickness (m)
η	Blasius similarity variable, $Y/(\nu X/U_\infty)^{1/2}$
θ	momentum thickness, $0.664X/Re_X^{1/2}$
θ_b	dimensionless basic temperature, $(T - T_\infty)/(T_w - T_\infty)$
λ	wave length in Z-direction (m)
μ	dynamic viscosity of fluid (kg-m/s)
ν	kinematic viscosity of fluid (m^2/s)
ξ	vorticity function in X-direction defined in (9) (1/s)
ψ	stream function (m^2/s)
τ	local wall stress

Superscripts

$*$	onset position

Subscripts

b	basic flow quantity
p	perturbation quantity

w	wall condition
X	local co-ordinate
δ_r	characteristic boundary layer thickness
∞	free stream condition

REFERENCES

1. Herbert T. On the stability of boundary layer along a concave wall. *Archives of Mechanics* 1976; **28**: 1039–1055.
2. Floryan JM. On the Goertler instability of boundary layers. *Progress in Aerospace Science* 1991; **28**: 235–271.
3. Aouidef A, Wesfried JE, Mutabaz I. Coriolis effects on Goertler vortices in the boundary layer flow on concave wall. *AIAA Journal* 1992; **30**(11):2779–2782.
4. Zebib A, Bottaro A. Goertler vortices with system rotation: linear theory. *Physics of Fluids A* 1993; **5**(5): 1206–1210.
5. Edo Y, Obi S, Masuda S. Heat transfer experiments in rotating boundary layer flow. *International Journal of Heat and Fluid Flow* 2000; **21**:684–692.
6. Hwang GJ, Lin MH. Estimation of the onset of longitudinal vortices in a laminar boundary layer heated from below. *ASME Journal of Heat Transfer* 1995; **117**:835–842.
7. Lin MH, Hwang GJ. Numerical study of the formation of longitudinal vortices in a laminar boundary layer with rotation. *Journal of the Chinese Society of Mechanical Engineers* 2000, **21**(4):341–349.
8. Mutabazi I, Normand C, Wesfreid JE. Gap size effects on centrifugally and rotationally driven instabilities. *Physical Review A*, 1992; **4**(6):1199–1205.
9. Matsson OJE, Alfredsson PH. Experiments on instabilities in a curved channel flow. *Physical Review A* 1992; **4**(8):1666–1676.
10. Selmi A, Nandakumar K, Finley WH. A bifurcation study of viscous flow through a rotating curved duct. *Journal of Fluid Mechanics* 1994; **262**:353–375.
11. Matsson OJE, Alfredsson PH. The effect of spanwise system rotation on dean vortices. *Journal of Fluid Mechanics* 1994; **274**:243–265.
12. Wang L, Cheng KC. Flows in curved channel with a low negative rotation speed. *Physical Review E* 1995; **51**:1155–1161.
13. Wang L. The effect of negative spanwise rotation on dean vortices. *ASME Journal of Fluids Engineering* 1997; **119**:718–721.
14. Tani I. Production of longitudinal vortices in the boundary layer along a concave wall. *Journal of Geophysical Research* 1962; **67**(8):3075–3080.
15. Wortmann FX. Visualization of transition. *Journal of Fluid Mechanics* 1969; **38**:473–480.
16. Bippes H. Experimental study of the laminar-turbulent transition of a concave wall in a parallel flow. *NASA* 1978; TM-75243.
17. Winoto SH, Durao DFG, Crane RI. Measurements within Goertler vortices. *ASME Journal of Fluids Engineering* 1979; **101**:517–520.
18. Swearingen JD, Blackwelder RF. The growth and breakdown of streamwise vortices in the presence of a wall. *Journal of Fluid Mechanics* 1987; **182**:255–290.
19. Peerhossaini H, Wesfreid JE. On the inner structure of streamwise Goertler rolls. *International Journal of Heat and Fluid Flow* 1988; **9**(1):12–18.
20. Lee SL. Weighting function scheme and its application on multidimensional conservation equations. *International Journal of Heat Mass Transfer* 1989; **32**:2065–2073.
21. Akiyama M, Hwang GJ, Cheng KC. Experiments on the onset of longitudinal vortices in laminar forced convection between horizontal plates. *ASME Journal of Heat Transfer* 1971; **93**:335–341.
22. Ostrach S, Kamontani Y. Heat transfer augmentation in laminar fully developed channel flow by means of heating from below. *ASME Journal of Heat Transfer* 1975; **97**:220–225.
23. Cheng KC, Kim YW. Vortex instability phenomena relating to the cooling of a horizontal isothermal flat-plate by natural and forced laminar convection flows. In *Cooling Technology for Electronic Equipment*, Aung W (ed.). Hemisphere: Washington, DC, 1988; 169–182.
24. Masuda S, Matubara M. Visual study of boundary layer transition on a rotating flat plate. *Third IUTAM Symposium on Laminar-Turbulent Transition*, Toulouse, France, 1989; 699–704.
25. Matsson OJE. Experiments on streamwise vortices in curved wall jet flow. *Physics of Fluids* 1995; **7**(12): 2978–2988.

26. Jean JF. Visualization of vortices in a rotating curved-rectangular passage. *Ms. Thesis*, National Tsing-Hwa University, Taiwan, ROC, 1997.
27. White FM. *Viscous Fluid Flow* (2nd edn). McGraw-Hill: New York, 1991; 378.
28. Bejan A. *Heat Transfer* (1st edn). John Wiley & Sons, Inc.: New York, 1993; 260.
29. Lin MH, Hwang GJ. Numerical prediction of the formation of Goertler vortices on a concave surface with suction and blowing. *International Journal for Numerical Methods in Fluids* 1999; **31**:1281–1295.

